

Hybrid LES-RANS modelling: a one-equation SGS model combined with a $k-\omega$ model for predicting recirculating flows

L. Davidson^{1,*} and S. H. Peng²

¹*Department of Thermo and Fluid Dynamics, Chalmers University of Technology, SE-412 96 Göteborg, Sweden*

²*FOI (Swedish Defence Research Agency), Aeronautics Division, SE-172 90 Stockholm, Sweden*

SUMMARY

A hybrid LES-RANS modelling approach is proposed. RANS is used in the near wall regions ($y^+ \lesssim 60$), and the turbulence is modelled with a $k-\omega$ model. LES is used in the remaining part of the flow, and the SGS turbulence is modelled with a one-equation k_{sgs} model. The same continuity and momentum equations are solved throughout the domain, the only difference being that the turbulent viscosity is taken from the $k-\omega$ model in the RANS region, and from the one-equation k_{sgs} model in the LES region. The new modelling approach is applied to two incompressible flow test cases. They are fully developed flow in a plane channel and the flow over a 2D-hill in a channel. Copyright © 2003 John Wiley & Sons, Ltd.

KEY WORDS: LES; hybrid models; zonal models; LES-RANS; DES

1. INTRODUCTION

In large eddy simulation (LES), a spatial-filtering is made either explicitly or implicitly to the turbulent flow field, where the filtered, large-scale motion is directly simulated, and the effect of subgrid-scale (SGS) motion is modelled. Traditional Reynolds-averaged Navier–Stokes (RANS) approaches do not attempt to resolve any flow structures, but model the effect of turbulence on the mean flow in terms of representative mean turbulence scales. As a result, all spectral effects are lost in the time averaging process. For many turbulent flows of engineering importance, indeed, traditional RANS modelling may be an awkward approach or even may fail to reproduce relevant flow physics. Examples include the flow past a bluff body that exhibits unsteadiness characterized by large, turbulent structures. By contrast, LES is viewed as a technique that is able to provide more comprehensive physical insight of such turbulent flows and thus produce in general more accurate predictions than traditional RANS approaches.

* Correspondence to: L. Davidson, Department of Thermo and Fluid Dynamics, Chalmers University of Technology, Hörsalsvägen 7, SE-412 96 Göteborg, Sweden.

† E-mail: lada@tfd.chalmers.se, <http://www.tfd.chalmers.se/~lada>

However, unlike in (unsteady) RANS computations where the mesh is refined only in the wall-normal direction, in a full LES a sufficiently refined grid resolution is required in all directions to account for near-wall flow structures in space. In LES the near-wall grid spacing should be about $y^+ \simeq 1$ in the wall-normal direction. This is similar to the requirement in RANS using low- Re number models. The requirement for a well-resolved LES on Δx^+ (streamwise) and Δz^+ (spanwise) in the near-wall region is approximately 100 and 20, respectively [1]. This enables resolution of the near-wall turbulent structures in the viscous sublayer and the buffer layer (streaks), which are responsible for the major part of the turbulence production. Thus, for wall-bounded flows at high Reynolds numbers of engineering interest, the computational resource requirement of accurate LES is prohibitively large [2]. Indeed, the requirement of near-wall grid resolution has largely deterred the application of LES in engineering practice. In spite of recent development of a number of advanced SGS models, see e.g. References [3–11], it should be recognized that the near-wall modelling has been a severe bottleneck problem to the introduction of advanced LES techniques in numerical analyses of industrial flow systems.

1.1. Near-wall modelling

In recognition of the necessity of efficient near-wall modelling in LES, in particular for turbulent flows at high Re numbers, several approaches have been proposed to alleviate the near-wall resolution requirement. These approaches developed so far may be divided into two categories: the wall-function approach, and the hybrid two-layer approach. The wall-function method employs a coarse mesh near the wall placing the first off-wall grid node outside the buffer layer in the boundary layer. This method usually uses some generalized wall laws, assuming that the wall stress is proportional to the velocity in the first grid node to replace the no-slip boundary condition. Such an approach was introduced by Schumann [12]. Similar methods were proposed and further improved by Grötzbach [13] and Piomelli *et al.* [14]. Although good agreement was reported when applied to simple plane channel flows, the validity of such methods is questionable for complex flows. Similar to the logarithmic law used by Mason and Gallen [15] and the power law adopted by Werner and Wengle [16], the assumption of a local stress equilibrium implied in the wall-function approaches is not valid for flows with separation. Bagwell *et al.* [17] proposed the use of linear stochastic estimation to approximate the wall shear stress and presented very accurate results for plane channel flow. However, this method requires *a priori* known two-point correlation tensor (from experiments or previous DNS), which is unrealistic for practical use.

In the category of hybrid two-layer approaches, the near-wall layer is computed using approximated model equations and coupled with LES in the off-wall outer (core) region. Two types of methodologies have been used in formulating the near-wall model. In the first type of methodology [18, 19], the turbulent boundary layer equations—employing a wall-damped, RANS-type eddy viscosity—are solved on an embedded mesh in the near-wall layer and, consequently, the computed wall stress is provided to the first LES off-wall grid node. No-slip wall boundary conditions is used for solving the boundary layer equations. While this approach works adequately in predicting mean flow statistics for attached flow, it performs poorly in separating and reattaching flow [20]. This method has lately been improved by computing the eddy-viscosity coefficient dynamically using information from the LES region [21–24].

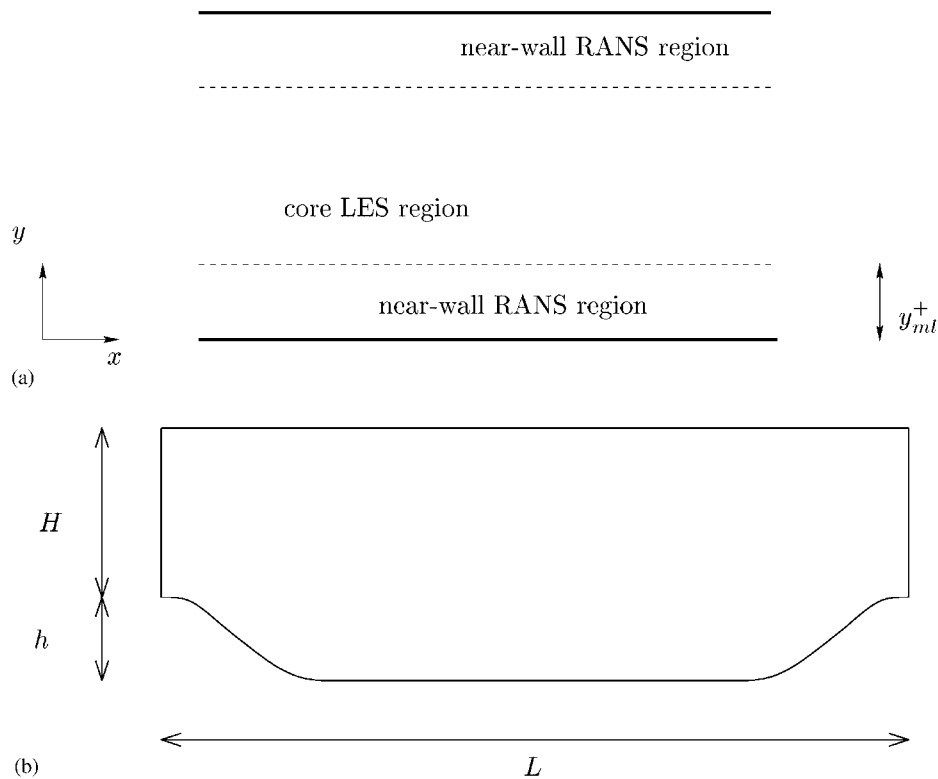


Figure 1. (a) The near-wall RANS region and the core LES region. (b) Hill-flow configuration. $h = 0.028$, $H = 0.057$, $L = 9h$, $z_{\max} = 9h$.

In the second type of the two-layer approach, the SGS modelling in the core region is supplemented with a full RANS transport model in the near-wall region of the wall, see Figure 1(a). The basic idea is to model the near-wall structure altogether in the context of unsteady RANS model so that the near-wall grid resolution in the directions parallel to the wall may largely be alleviated (and thus also the time-step constraint is relaxed). This method is in the present work called a hybrid LES-RANS method. Among others, the detached eddy simulation (DES) proposed by Spalart *et al.* [2] has probably drawn the most attention in the past years. In DES the one-equation Spalart–Allmaras (S-A) RANS eddy viscosity model is used in the near-wall region, and the length scale in the model is switched to the local grid spacing in the core regions, where the model turns into a one-equation SGS model. The practical reasoning of using DES lies in the argument that a fine-tuned RANS model is able to give reasonable predictions for attached boundary layer, while LES is powerful to account for separated regions. The reason for this is that it is easy to resolve massively separated flows, where the dominated turbulent scales are large. On the contrary, the dominating turbulent scales in boundary layers (the streaks) are much smaller, and they scale with the wall parameters (inner scaling). Indeed, a number of successful applications of DES have been reported for flows with massive separation, see e.g. References [25–29]. A dramatic reduction

in computational cost comparing to a full LES was also reported in simulations for high- Re number flows around a wing [25, 29]. In spite of its encouraging performance for massively separated flows, DES for attached flows, e.g. channel flows [30], shows a fairly strong dependency on the grid arrangement in the wall-parallel directions. In References [31, 32] a hybrid LES-RANS methodology is employed in which a one-equation model is used both in the near-wall region and in the core region. The length scale in the near-wall region is related to the wall distance and the length scale is proportional to the control volume size. Good results are presented for both fully developed channel flow and for the flow in a ribbed channel.

In this work a hybrid modelling approach is proposed using a two-equation $k-\omega$ model in the near-wall region (the RANS region) combined with a one-equation k_{sgs} model in the core region (the LES region), see Figure 1(a). To model the turbulent transport in the momentum equation, the turbulent RANS viscosity from the $k-\omega$ model is used in the RANS region, and the turbulent SGS viscosity from the one-equation model is used in the LES region. Coarse grid spacing is used in grid planes parallel to the walls. This is the main reason why hybrid LES-RANS is much cheaper than LES. For simplicity, the matching plane between the RANS and LES region is presently defined at a pre-selected grid plane, which is located in the logarithmic part of the boundary layer, i.e. in the fully turbulent region. In the logarithmic region coarse grid spacing in planes parallel to the wall (Δx and Δz) is adequate for LES, because the grid spacings are dictated by the requirement of resolving the mean flow rather than the near-wall turbulent processes.

The present hybrid LES-RANS approach is in a way similar to DES. One difference is that in DES the object is to model the entire turbulent boundary layer with RANS; only the detached eddies in the outer boundary layer are modelled with LES. In the present hybrid LES-RANS, the matching plane is located somewhere in the logarithmic part of the boundary layer.

The paper is organized as follows. In the next section equations, turbulence models and the numerical method are described. In the following section, results are presented and discussed, and conclusion are drawn in the final section.

2. THE MODELLING METHODOLOGY

2.1. Equations

The Navier–Stokes equation, time-averaged in the near-wall regions and filtered in the core region, reads

$$\frac{\partial \bar{u}_i}{\partial t} + \frac{\partial}{\partial x_j} (\bar{u}_i \bar{u}_j) = \beta \delta_{1i} - \frac{1}{\rho} \frac{\partial \bar{p}}{\partial x_i} + \frac{\partial}{\partial x_j} \left[(v + v_T) \frac{\partial \bar{u}_i}{\partial x_j} \right] \quad (1)$$

$$\frac{\partial \bar{u}_i}{\partial x_i} = 0 \quad (2)$$

where $v_T = v_t$ (v_t denotes the turbulent RANS viscosity) for $y \leq y_{\text{ml}}$ (see Figure 1(a)), otherwise $v_T = v_{\text{sgs}}$. The first term on the right-hand side of Equation (1) represents the streamwise driving pressure gradient term, both in the channel flow and the hill flow. In the former case

the Reynolds number based on the wall-friction velocity Re_τ is prescribed, and thus $\beta = 1$. For the hill flow, in order to get the correct bulk flow rate different values of β were tested. A value of $\beta = 1$ was finally chosen which is kept constant in all hill computations.

For both the channel flow and the hill flow, periodic boundary conditions are used in the streamwise and spanwise directions. No slip conditions are used at the walls in the channel flow, and at the lower wall in the hill flow. At the upper hill flow wall, because the resolution is here rather poor ($y^+ \approx 30$ for the first node), the log-law wall functions is used (no RANS region is used here).

The bar ($\bar{\cdot}$) over the velocity components and pressure in Equations (1) and (2) denotes time averaging in the RANS region and filtering (volume averaging) in the LES region. Thus the flow variables in the RANS region and in the LES region are defined in different ways. When advection of, for example, momentum takes place across the matching plane from the LES region to the RANS region, a filtered (i.e. volume averaged) velocity is transported into a region in which the momentum equations are defined by time-averaging. This is somewhat inconsistent. Nevertheless, if we view the unsteady RANS as a very large eddy simulation (VLES) in which the flow variables are filtered using a large filtering length scale (equivalent to the RANS-defined turbulent length scale), consistency is retained. In other words, the alternative interpretation is that filtering is employed in both the RANS and LES regions, but with different length scales. The SGS length scale in the near-wall region is defined from k and ω , and in the core region from the cell size. More discussion is given in Section 3.3.

2.2. The hybrid LES-RANS model

A low-Reynolds number k - ω model [33] is used in the near-wall layer, and the one-equation SGS model by Yoshizawa [34] in the core region. The k - ω model is formulated as

$$\begin{aligned} \frac{\partial k}{\partial t} + \frac{\partial}{\partial x_j}(\bar{u}_j k) &= \frac{\partial}{\partial x_j} \left[\left(v + \frac{v_t}{\sigma_k} \right) \frac{\partial k}{\partial x_j} \right] + P_k - c_k f_k \omega k \\ \frac{\partial \omega}{\partial t} + \frac{\partial}{\partial x_j}(\bar{u}_j \omega) &= \frac{\partial}{\partial x_j} \left[\left(v + \frac{v_t}{\sigma_\omega} \right) \frac{\partial \omega}{\partial x_j} \right] + \frac{\omega}{k} (c_{\omega 1} f_\omega P_k - c_{\omega 2} k \omega) + c_\omega \frac{v_t}{k} \left(\frac{\partial k}{\partial x_j} \frac{\partial \omega}{\partial x_j} \right) \\ v_t &= f_\mu \frac{k}{\omega}, \quad P_k = 2 v_t \bar{S}_{ij} \bar{S}_{ij}, \quad \bar{S}_{ij} = \frac{1}{2} \left(\frac{\partial \bar{u}_i}{\partial x_j} + \frac{\partial \bar{u}_j}{\partial x_i} \right) \\ f_\mu &= 0.025 + \left\{ 1 - \exp \left[- \left(\frac{R_t}{10} \right)^{3/4} \right] \right\} \left\{ 0.975 + \frac{0.001}{R_t} \exp \left[- \left(\frac{R_t}{200} \right)^2 \right] \right\} \\ f_\omega &= 1 + 4.3 \exp \left[- \left(\frac{R_t}{1.5} \right)^{1/2} \right], \quad f_k = 1 - 0.722 \exp \left[- \left(\frac{R_t}{10} \right)^4 \right] \\ c_k &= 0.09, \quad c_{\omega 1} = 0.42, \quad c_{\omega 2} = 0.075, \quad c_\omega = 0.75, \quad \sigma_k = 0.8, \quad \sigma_\omega = 1.35 \end{aligned} \tag{3}$$

The SGS model of Yoshizawa reads

$$\begin{aligned} \frac{\partial k_{\text{sgs}}}{\partial t} + \frac{\partial}{\partial x_j}(\bar{u}_j k_{\text{sgs}}) &= \frac{\partial}{\partial x_j} \left[(v + v_{\text{sgs}}) \frac{\partial k_{\text{sgs}}}{\partial x_j} \right] + P_{k_{\text{sgs}}} - C_\varepsilon \frac{k_{\text{sgs}}^{3/2}}{\Delta} \\ v_{\text{sgs}} &= C_k \Delta k_{\text{sgs}}^{1/2}, \quad P_{k_{\text{sgs}}} = 2v_{\text{sgs}} \bar{S}_{ij} \bar{S}_{ij} \end{aligned} \quad (4)$$

$$\Delta = \min \{ \Delta_\xi, \Delta_\eta, \Delta_\zeta \}, \quad C_k = 0.07, \quad C_\varepsilon = 1.05$$

where ξ, η and ζ denote the three co-ordinate directions defined by a general curvilinear grid. The turbulent kinetic energy in the RANS region ($y \leq y_{\text{ml}}$) is denoted by k , and the SGS turbulent kinetic energy in the LES region ($y > y_{\text{ml}}$) by k_{sgs} . The coefficients in the k_{sgs} equation have been slightly modified [35]. Contrary to the standard Yoshizawa model, in which $\Delta = (\Delta_\xi \Delta_\eta \Delta_\zeta)^{1/3}$, here the smallest cell side is used. This was found to considerably improve the channel flow predictions.

The matching plane near the wall is located at y_{ml} (see Figure 1(a)). The subscript j_{match} is used here to denote the cell below the matching plane y_{ml} , for which the following interface condition is used for ω :

$$j = j_{\text{match}}: \quad \frac{\partial \omega}{\partial y} = 0 \quad (5)$$

Contrary to the implementation in Reference [36], no interface condition is used for k and k_{sgs} . These quantities are simply transported by convection-diffusion over the matching plane.

2.3. The numerical method

An implicit, two-step time-advancement method is used. The discrete form of Equation (1) can be written as

$$\bar{u}_i^{n+1/2} = \bar{u}_i^n + \Delta t H(\bar{u}_i^n, \bar{u}_i^{n+1/2}) - \frac{1}{\rho} \alpha \Delta t \frac{\partial p^{n+1}}{\partial x_i} - \frac{1}{\rho} (1 - \alpha) \Delta t \frac{\partial p^n}{\partial x_i} \quad (6)$$

where $H(\bar{u}_i^n, \bar{u}_i^{n+1/2})$ includes the convection term and the viscous and SGS stresses, and $\alpha = 0.5$ (the Crank–Nicolson scheme). Equation (6) gives $\bar{u}_i^{n+1/2}$ which does not satisfy continuity. An intermediate velocity field is computed by subtracting the implicit part of the pressure gradient, i.e.

$$\bar{u}_i^* = \bar{u}_i^{n+1/2} + \frac{1}{\rho} \alpha \Delta t \frac{\partial p^{n+1}}{\partial x_i} \quad (7)$$

Now $\bar{u}_i^{n+1/2}$ in Equation (7) is replaced by the velocity field at level $(n+1)$, i.e. \bar{u}_i^{n+1} . Taking the divergence of Equation (7) and requiring that the face velocities $\bar{u}_{i,f}^{n+1}$ (which are obtained by linear interpolation) satisfy the continuity equation the following Poisson equation for pressure is obtained

$$\frac{\partial^2 p^{n+1}}{\partial x_i \partial x_i} = \frac{\rho}{\Delta t \alpha} \frac{\partial \bar{u}_{i,f}^*}{\partial x_i} \quad (8)$$

The numerical procedure at each time step is summarized as follows:

1. Solve the discretized Navier–Stokes equations for \bar{u} , \bar{v} and \bar{w} .
2. Create an intermediate velocity field \bar{u}_i^* from Equation (7).
3. The Poisson equation (Equation (8)) is solved with an efficient multigrid method [37].
4. Compute the face velocities $\bar{u}_{i,f}^{n+1}$ (which satisfy continuity) from the pressure and the intermediate velocity using

$$\bar{u}_{i,f}^{n+1} = \bar{u}_{i,f}^* - \frac{1}{\rho} \alpha \Delta t \left(\frac{\partial p^{n+1}}{\partial x_i} \right)_f \quad (9)$$

5. Solve the discretized k_T and ω equations.
6. The turbulent viscosity is computed.
7. Step 1 to 6 are iteratively performed until convergence (one or two iterations) is reached.
8. Next time step.

Note that an implicit dissipation is present which prevents odd-even decoupling. The intermediate velocity field is computed at the *nodes* (see Equation (7)) by subtracting a pressure gradient. Then, after having solved the pressure Poisson equation, the face velocity field is computed by adding a pressure gradient at the *faces* (see Equation (9)). As a consequence of these two steps (Steps 2 and 4) a term is implicitly added, which is the difference between the pressure gradient at the face and the node. It can readily be shown that this term is proportional to the third derivative of pressure, i.e. $\partial^3 p / \partial x_i^3$ [38], which is similar to the Rhie-Chow dissipation [39].

3. RESULTS

Below the two quantities v_T and k_T are frequently used. They are defined as follows: for $y \leq y_{ml}$, $v_T = v_t$, $k_T = k$, otherwise $v_T = v_{sgs}$, $k_T = k_{sgs}$.

3.1. Channel flow

Figure 2(a) shows the predicted $\langle \bar{u} \rangle$ velocity ($\langle \cdot \rangle$ denotes averaging over x , z and t) for fairly coarse meshes, see Table I. A $32 \times 64 \times 32$ (x, y, z) grid is used. It can be seen that for Case 2, in which the matching plane is located at $y^+ = 60$, and $\Delta z^+ = 104$, reasonable agreement with the well-resolved LES by Piomelli [40] is obtained. However, a small kink is visible near the location of the matching plane. When the resolution is made coarser in the spanwise direction (Case 3) the agreement with the benchmark LES becomes somewhat poorer in the LES region than in Case 2. Note that the grid for Case 1, 2 & 3 is much coarser than that required for a wall-resolved LES. Consequently, when only LES is used (Case 4), the results are much poorer than those obtained with the hybrid LES–RANS model.

Figure 2(b) presents the predicted resolved velocities fluctuations. The agreement with the benchmark LES is not good. The predictions are typical of an under-resolved LES: the stream-wise fluctuations are too large. It should be noted that the resolved stresses are large even in the RANS region ($y/\delta < 0.057$).

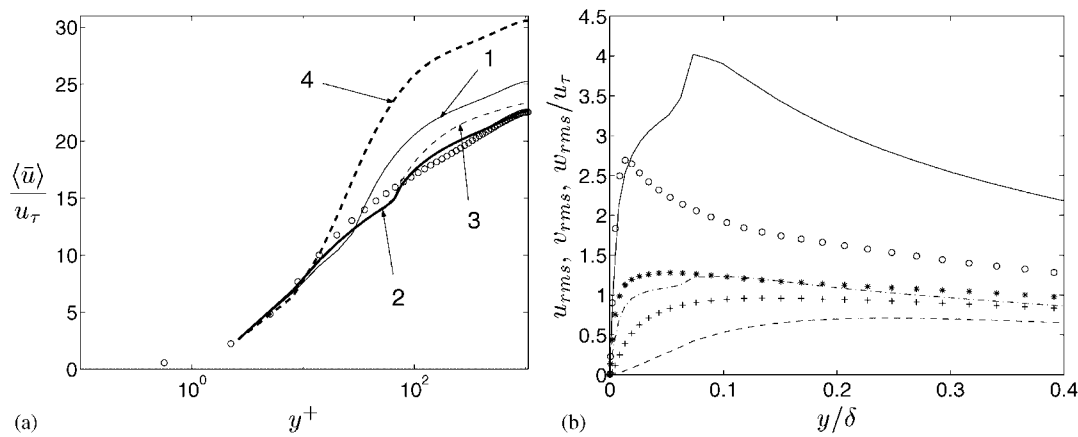


Figure 2. Channel flow. Markers: benchmark LES [40]: (a) Thin solid line: Case 1; thick solid line: Case 2; thin dashed line: Case 3; thick dashed line: Case 4; (b) Case 2. Resolved velocity fluctuations. Solid line: u_{rms} ; dashed line: v_{rms} ; dash-dotted line: w_{rms} .

Table I. Channel flow, $Re_\tau = u_\tau \delta / \nu = 1050$ (δ denotes half channel width), $x_{max} = 4\pi\delta$ ($\Delta x^+ = 412$). A $32 \times 64 \times 32$ (x, y, z) grid is used for all cases. Size of the computational domain and position of the matching plane (y_{ml}) between the LES and RANS regions. The j_{match} value represents number of cells in the RANS region at each wall. Note that only LES is used in Case 4.

Case	$z_{max}\delta$	y_{ml}/δ	j_{match}	y_{ml}^+	Δz^+
1	π	0.023	4	25	104
2	π	0.057	8	60	104
3	2π	0.057	8	60	208
4	π	0	0	0	104

3.2. Hill flow

The configuration of the hill flow is shown in Figure 1(b). A $104 \times 64 \times 32$ (x, y, z) grid is used. The matching plane along the lower wall is fixed to grid line number 13, so that the location of the matching plane is at $\langle n_{ml} \rangle / h = 0.1 \pm 0.02$. The cell size in the x and z directions together with the location of the matching plane (all in wall units) are shown in Figure 3. As can be seen, high local values in $\langle \Delta x^+ \rangle$ and $\langle \Delta z^+ \rangle$ occur above the crest, while $\langle \Delta x^+ \rangle \simeq \langle n_{ml}^+ \rangle \lesssim 30$ and $\langle \Delta z^+ \rangle \lesssim 80$ in the rest of the flow domain. For the nodes adjacent to the lower wall $\langle y^+ \rangle \lesssim 2$. The predictions are compared with a benchmark, wall-resolved LES [41, 42] in which more than 5 million cells were employed. Wall-resolved LES on this geometry was recently performed also by Temmerman and Leschziner [43] confirming the results in References [41, 42]. The Reynolds number based on the channel height and the channel bulk velocity is 21 500. Note that this is lower than what was used in References [36, 44].

Figures 4 and 5 compare the predicted $\langle \bar{u} \rangle$ velocity ($\langle \cdot \rangle$ denotes here averaging over z and t) and resolved velocity fluctuations with the benchmark LES. The agreement is fairly good. As

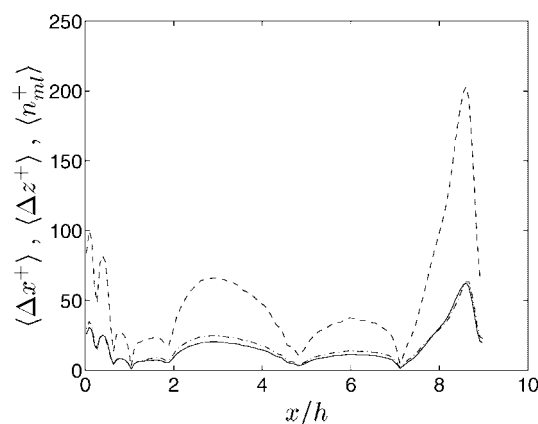


Figure 3. Hill flow. Grid spacing and location of matching plane. Solid line: $\langle \Delta x^+ \rangle$; dashed line: $\langle \Delta z^+ \rangle$; dash-dotted line: $\langle n_{ml}^+ \rangle$.

can be seen from the profile at $x = 2h$, the backflow with the hybrid LES-RANS model is slightly too strong. However, this is probably not due to the near-wall treatment. Instead it is believed to be a result of the shear layer emanating from the top of the hill being insufficiently resolved. Very small kinks are seen in the $\langle \bar{u} \rangle$ profiles close to the location of the matching plane, but are much less visible than found in the channel flow (cf. Figure 2). The reason for this is probably that in the hill flow, the convective and diffusive transport across the matching plane is considerable, which has a smoothening effect on the flow quantities.

3.3. Discussion

The turbulent RANS/SGS viscosities are shown in Figures 6(a) and 7(a). It can be seen that the turbulent RANS viscosities are large in the RANS region—much larger than is normally found in LES. Near the matching plane, ν_{sgs} in the LES region drops down to typical SGS values of $\langle \nu_{sgs} \rangle / \nu \leq 2$ for both channel and hill flows. The maximum value of ν_t for channel flow (Figure 6(a)) in the RANS region, which occurs near the matching plane, is $\langle \nu_{t,max} \rangle / \nu \simeq 9$. When 1D, steady RANS is used to compute the channel flow using the same grid and the same $k-\omega$ model, the value of ν_t at the same location is approximately twice as large. One of the reasons why the RANS calculation gives larger ν_t values than the hybrid LES-RANS, is that in the latter case more modelled turbulent kinetic energy is diffused from the near-wall region to the core region because k is reduced as $k \rightarrow k_{sgs}$ in the LES region (see Figure 6(b)). Another reason is that in the hybrid LES-RANS computations, a substantial part of the turbulence in the RANS region is accounted for by resolved turbulence, see Figures 2(b) and 6(b).

Figures 6(b) and 7(b) show the modelled turbulent RANS/SGS kinetic energy. For the channel flow (Figure 6(b)), the modelled RANS kinetic energy agrees well with the benchmark values. However, the resolved kinetic energy is as large as the modelled one in the RANS region. Therefore, the total kinetic energy (sum of modelled and resolved) is much too large. This is, as also noted in Reference [45], a fundamental problem in hybrid LES-RANS. In the hill flow (Figure 7(b)), the turbulent RANS kinetic energy is not that large. When a 2D

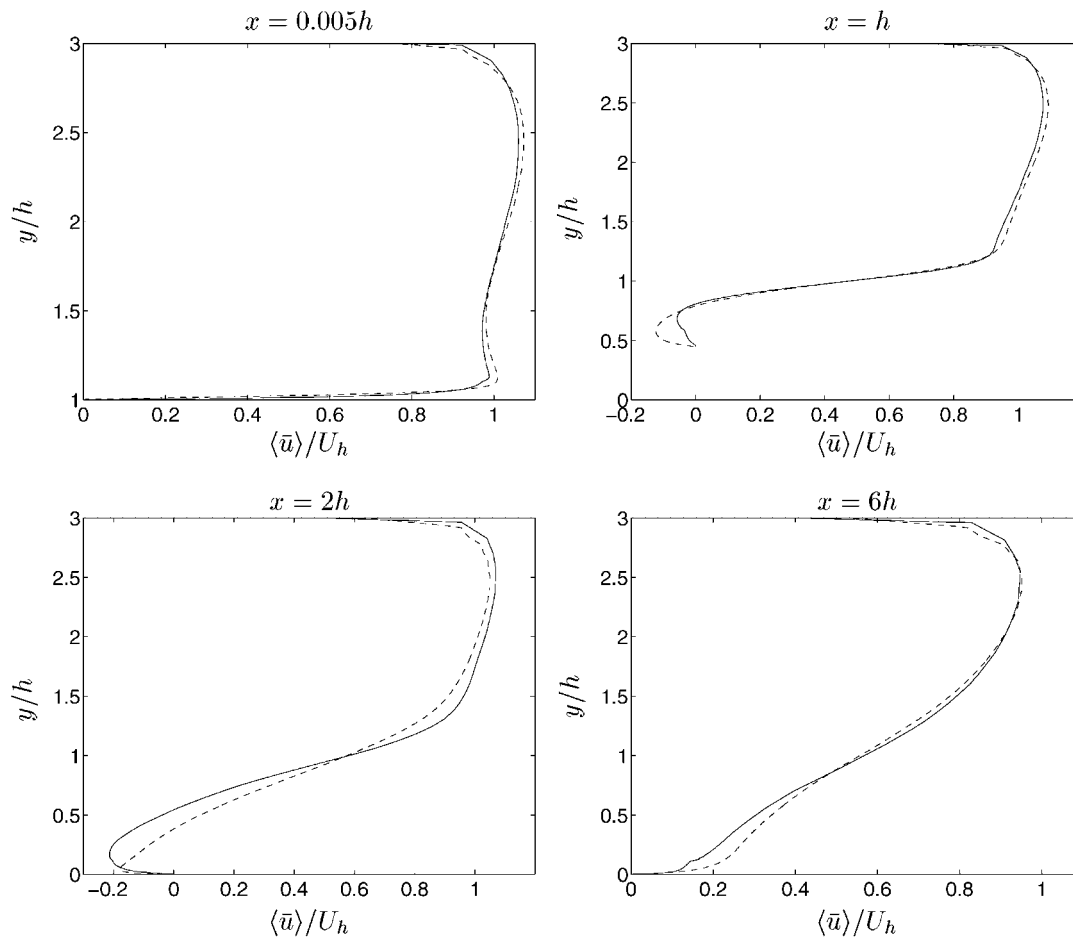


Figure 4. Hill flow. $\langle \bar{u} \rangle$ profiles. U_h denotes the bulk velocity at the crest of the hill (i.e. at $x=0$ and $x=L$). Solid lines: hybrid LES-RANS; dashed lines: benchmark LES [41, 42].

RANS computation is performed with the same grid and the same $k-\omega$ model, the modelled turbulent kinetic energy is up to 50% larger compared to the hybrid LES-RANS data in Figure 7(b), but still smaller than the benchmark data. The reason why k is higher in a 2D RANS computation is, as in the channel flow computations, that less turbulent kinetic energy is diffused from the near-wall region to the core region.

Figures 8(a) and 9(a) depict the modelled turbulent length scales. The modelled turbulent RANS/SGS viscosity can be defined as $\nu_T \propto \mathcal{U}\ell$, where \mathcal{U} and ℓ represent the turbulent RANS (SGS) velocity scale and length scale in the RANS (LES) region, respectively. In the LES region, the SGS length scale is estimated by $\ell \equiv \Delta = \nu_{\text{sgs}}/(C_k k_{\text{sgs}}^{1/2})$, see Equation (4). In order to compare the turbulent RANS and the SGS length scales, the turbulent length scale in the RANS region is defined in the same way, so that $\ell = \nu_T/(C_k k_T^{1/2})$ in both the RANS and the LES region. As can be seen in Figures 8(a) and 9(a), the turbulent RANS/SGS length

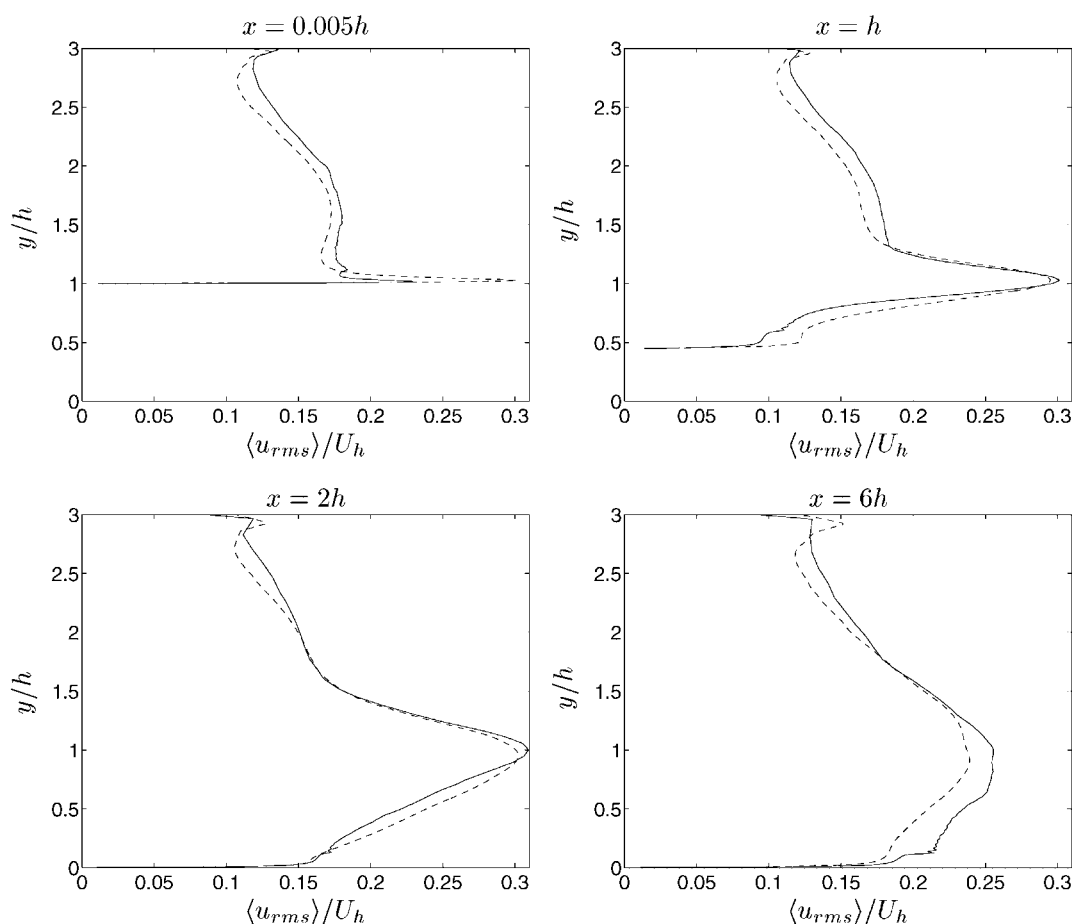


Figure 5. Hill flow. Resolved $\langle u_{rms} \rangle$ profiles. Solid lines: hybrid LES-RANS; dashed lines: benchmark LES [41, 42].

scale decreases steeply from the RANS region to the LES region. This is the main reason for the decrease in the turbulent viscosity (Figures 6(a) and 7(a)) and the RANS/SGS turbulent kinetic energy (Figures 6(b) and 7(b)).

In unsteady RANS, there should be a scale separation between the modelled time scale, T_{mod} , and the resolved time scale, T_{res} , so that $T_{mod} \ll T_{res}$. In the RANS region, the turbulent viscosity is computed as $\nu_t = k/\omega$, and thus the modelled time scale can be defined as $T_{mod} = 1/\omega$. The smallest resolved time scale is related to the smallest resolved length scale, and it can be defined as $T_{res} = \min\{\Delta_\xi, \Delta_\eta, \Delta_\zeta\} / \langle k_{res} \rangle^{1/2} = \Delta / \langle k_{res} \rangle^{1/2}$, where k_{res} is the resolved turbulent kinetic energy. The modelled and the resolved time scales are compared in Figures 8(b) and 9(b). Two time scales in the RANS region representative of the modelled turbulence are presented in Figures 8(b), namely $1/\omega$ and $1/|\bar{S}|$ ($|\bar{S}| = (2\bar{S}_{ij}\bar{S}_{ij})^{1/2}$). As can be seen, the modelled time scale close to the wall is indeed smaller than the resolved one. However, in a large part of the RANS region, the situation is the reverse: the modelled time

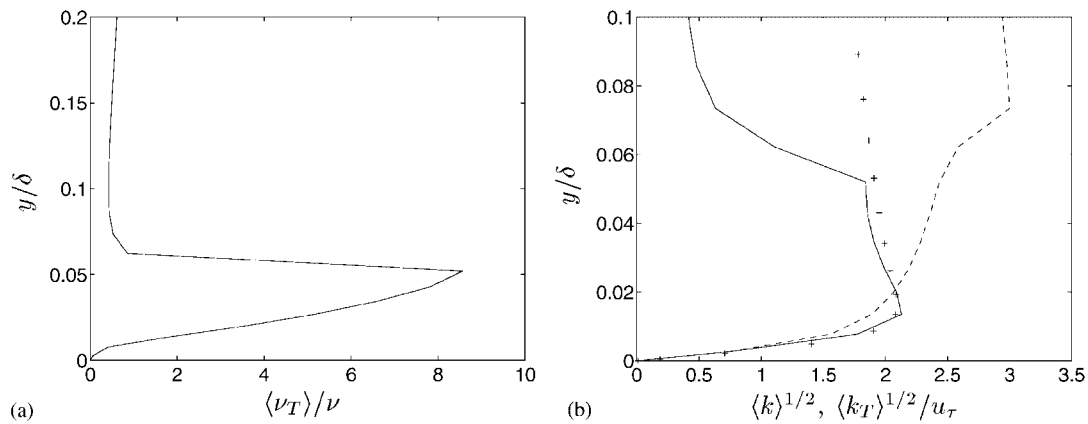


Figure 6. Channel flow, Case 2. Near-wall region. Turbulent RANS/SGS viscosity and modelled turbulent RANS/SGS kinetic energy. (a) RANS/SGS turbulent viscosity. (b) Solid line: modelled turbulent RANS/SGS kinetic energy; dashed line: resolved turbulent kinetic energy; markers: benchmark LES [40].

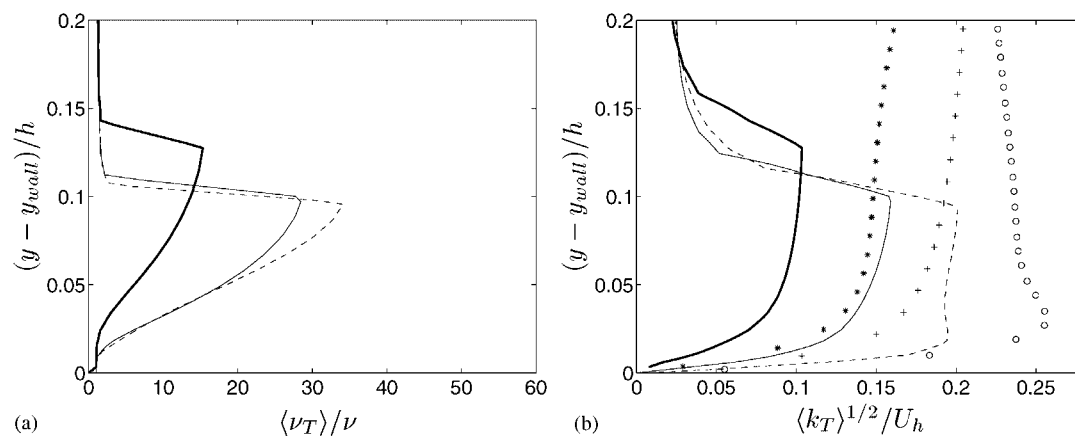


Figure 7. Hill flow. Near-wall region. Dashed line, o: $x/h = 0.005$; thick solid line, *: $x/h = 1$; thin solid line, +: $x/h = 6$. Markers: resolved turbulence from benchmark LES [41, 42]: (a) Turbulent RANS/SGS viscosity. (b) Modelled turbulent RANS/SGS kinetic energy.

scale is *larger* than the resolved one. Thus, scale separation between modelled and resolved turbulence does not exist, and the unsteady RANS performed in the near-wall is formally not correct. Indeed, it would be more appropriate to denote the near-wall region a VLES region. The SGS length scale in the VLES region is then $\ell = \nu_t / (C_k k^{1/2})$, which is presented in Figures 8(a) and 9(a). Note that if the near-wall region is defined as a VLES region, it does not have any implications in the finite volume code: *it remains the same*.

There may also be some questions in defining the near-wall region as a VLES region. In this case, it may well happen that our SGS length scale, ℓ , becomes much larger than

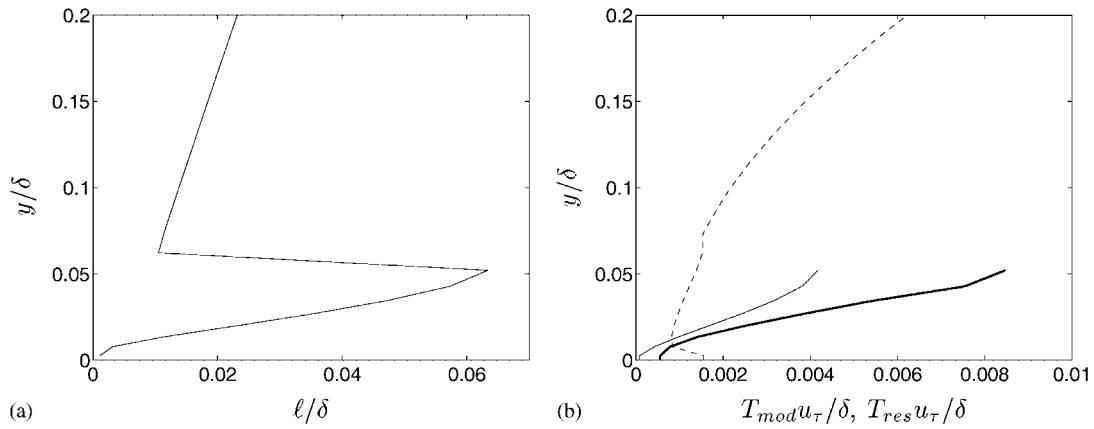


Figure 8. Channel flow, Case 2. Near-wall region. Turbulent RANS/SGS length scale and turbulent RANS/SGS time scales: (a) RANS/SGS turbulent length scale, $\ell = \langle v_T \rangle / (C_k \langle k_T \rangle^{1/2})$. (b) Solid thin line: modelled turbulent time scale $u_\tau / (\delta \langle \omega \rangle)$; solid thick line: $u_\tau / (\delta |\bar{S}|)$; dashed line: resolved turbulent time scale $u_\tau \Delta / (\delta \langle k_{res} \rangle^{1/2})$.

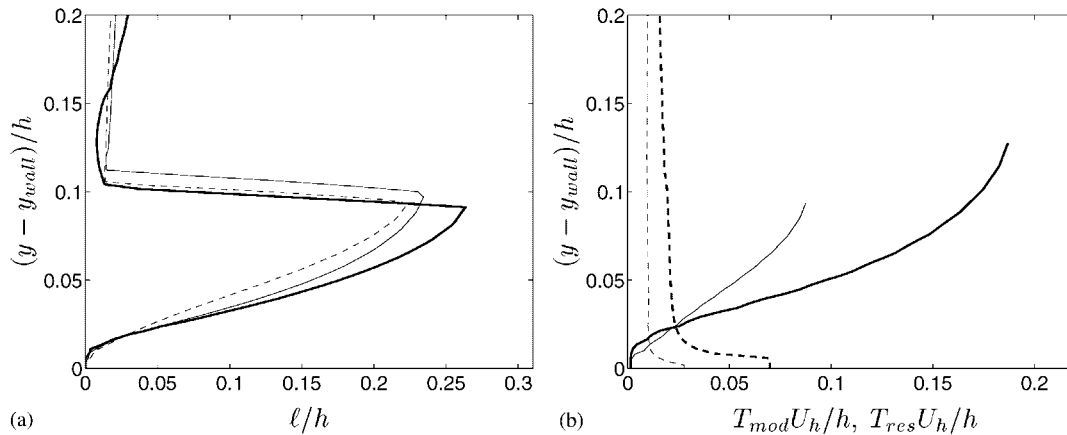


Figure 9. Hill flow. Near-wall region. Turbulent RANS/SGS length scale and turbulent RANS/SGS time scales: (a) Turbulent modelled length scale $\ell = \langle v_T \rangle / (C_k \langle k_T \rangle^{1/2})$. Dashed line: $x/h = 0.005$; thick solid line: $x/h = 1$; thin solid line: $x/h = 6$. (b) Solid lines: modelled turbulent time scale $U_h / (h \langle \omega \rangle)$; dashed lines: resolved turbulent time scale $U_h \Delta / (h \langle k_{res} \rangle^{1/2})$. Thin lines: $x/h = 0.005$; thick lines: $x/h = 1$.

the filter size, Δ . Is that acceptable? The answer is probably that it depends on *how* much larger. In the Smagorinsky models, the SGS length scale is in the literature usually chosen as the cubic root of the cell volume. Near walls this is much larger than the smallest cell side. However, if the SGS length scale in the VLES region becomes *very much* larger than Δ , it may be necessary to increase the filter size through explicit filtering. This adds high complexity to the computations, especially since Δ would in general not be an even multiple of any cell width, i.e. $\Delta \neq q \min\{\Delta_\xi, \Delta_\eta, \Delta_\zeta\}$ where q is an integer. A further complication

is that the filter width would be a function not only of the space coordinates but also of time, i.e. $\Delta = \Delta(x_i, t)$. Thus there would appear a commutation error in the time-derivative term in all equations, because the filter function would be a function of both space and time, i.e. $G = G(x_i, t)$. However, this error would probably be negligible in the same way as the commutation error due to non-constant filter size in space is negligible [46].

4. CONCLUSIONS

A hybrid LES-RANS model is presented. In the near-wall region, unsteady RANS is used and the turbulence is modelled with a $k-\omega$ model. LES is used in the core region and the SGS turbulence is modelled with a one-equation SGS model. The matching plane is fixed along a pre-selected grid plane in the inner part of the logarithmic region. The main idea is to avoid resolving the near-wall streaks in the viscous and the buffer layer and thereby avoiding the necessity of using a fine grid in the wall-parallel plane. Instead these near-wall structures are modelled in the same way as in RANS. However, the large turbulent scales in the core region ($y^+ \gtrsim 60$) are resolved by the LES.

The hybrid LES-RANS model has been applied to a fully developed channel flow and a hill flow. The mean flow is fairly well predicted with a coarse mesh, both for the channel flow and the hill flow. Kinks in the velocity profiles are observed in the region of the matching plane. However, this problem is much smaller in the hill flow. The reason is probably that the transport of mass and momentum across the matching plane by convection and turbulent diffusion has a smoothing effect. One way to further reduce the gradients across the matching plane could be to use some kind of smoothing function as proposed by Strelets [29].

One major problem with the hybrid LES-RANS approach, is that the flow provided by the unsteady RANS to the LES region across the matching plane does not have proper spectral properties. Although the unsteady RANS equations do predict some resolved time and length scales, they are not relevant for the LES-resolved turbulence. Thus the LES region in the core region is supplied by very poor information from the RANS region. In on-going work [47, 48], resolved turbulent fluctuations u' , v' , w' (taken from a channel DNS and scaled with k) are superimposed on the RANS velocities \bar{u} , \bar{v} , \bar{w} at the matching plane. This approach has been tested for channel flow and the flow in a asymmetric diffuser, and the results are very promising.

ACKNOWLEDGEMENTS

Computer time at the SGI ORIGIN 2000 machines at UNICC, Chalmers, is gratefully acknowledged.

REFERENCES

1. Piomelli U, Chasnov JR. Large-eddy simulations: theory and applications. In *Transition and Turbulence Modelling*, Henningson D, Hallbäck M, Alfredsson H, Johansson A (eds). Kluwer Academic Publishers: Dordrecht, 1996; 269–336.
2. Spalart PR, Jou W-H, Strelets M, Allmaras SR. Comments on the feasibility of LES for wings and on a hybrid RANS/LES approach. In *Advances in LES/DNS, First International Conference on DNS/LES*, Liu C, Liu Z (eds). Greyden Press, Louisiana Tech University: Ruston, LA, 1997.
3. Germano M, Piomelli U, Moin P, Cabot WH. A dynamic subgrid-scale eddy viscosity model. *Physics of Fluids A* 1991; **3**:1760–1765.

4. Zang Y, Street RL, Koseff JR. A dynamic mixed subgrid-scale model and its application to turbulent recirculating flows. *Physics of Fluids A* 1993; **5**:3186–3196.
5. Ghosal S, Lund TS, Moin P, Akselvoll K. A dynamic localization model for large-eddy simulation of turbulent flows. *Journal of Fluid Mechanics* 1995; **286**:229–255.
6. Ghosal S, Lund TS, Moin P, Akselvoll K. Corrigendum. *Journal of Fluid Mechanics* 1995; **297**:402.
7. Meneveau C, Lund T, Cabot W. A Lagrangian dynamic model subgrid-scale model of turbulence. *Journal of Fluid Mechanics* 1996; **315**:353–385.
8. Davidson L. Large eddy simulation: A dynamic one-equation subgrid model for three-dimensional recirculating flow. In *11th International Symposium on Turbulent Shear Flow*, vol. 3, Grenoble, 1997; 26.1–26.6.
9. Domaradzki JA, Loh KC. The subgrid-scale estimation model in the physical space representation. *Physics of Fluids A* 1999; **11**:2330–2338.
10. Porté-Agel F, Meneveau C, Parlange MB. A scale-dependent dynamic model for large-eddy simulation: Application to a neutral atmospheric boundary layer. *Journal of Fluid Mechanics* 2000; **415**:261–284.
11. Krajnović S, Davidson L. A mixed one-equation subgrid model for large-eddy simulation. *International Journal of Heat and Fluid Flow* 2002; **23**(4):413–425.
12. Schumann U. Subgrid scale model for finite difference simulations of turbulent flows in plane channels and annuli. *Journal of Computational Physics* 1975; **18**:376–404.
13. Grötzbach G. Direct numerical and large eddy simulation of turbulent channel flow. *Encyclopedia of Fluid Dynamics* 1987; **6**:1337–1397.
14. Piomelli U, Ferziger J, Moin P. New approximate boundary conditions for large eddy simulations. *Physics of Fluids A* 1989; **1**:1061–1068.
15. Mason PJ, Callen NS. On the magnitude of the subgrid-scale eddy coefficient in large-eddy simulations of turbulent channel flow. *Journal of Fluid Mechanics* 1986; **162**:439–462.
16. Werner H, Wengle H. Large-eddy simulation of turbulent flow over and around a cube in a plane channel. In *Turbulent Shear Flows*, vol. 8. Springer: Berlin, 1991; 155–168.
17. Bagwell G, Andrian RJ, Moser RD, Kim J. Improved approximation of wall shear stress boundary conditions for large eddy simulation. In *Near Wall Turbulence Flows*, Speziale CG, Launder BE (eds). Elsevier Science: Amsterdam, 1993; 265–275.
18. Cabot W. Large-eddy simulations with wall models. In *Annual Research Briefs*, Center for Turbulent Research, Stanford Univ./NASA Ames Research Center, 1995; 41–50.
19. Balaras E, Benocci C, Piomelli U. Two-layer approximate boundary conditions for large-eddy simulations. *AIAA Journal* 1996; **34**:1111–1119.
20. Cabot W. Wall models in large eddy simulations of separated flow. In *Annual Research Briefs*, Center for Turbulent Research, Stanford Univ./NASA Ames Research Center, 1997; 97–106.
21. Cabot W. Near-wall models in large eddy simulations of flow behind a backward-facing step. In *Annual Research Briefs*, Center for Turbulent Research, Stanford Univ./NASA Ames Research Center, 1996; 199–210.
22. Cabot W, Moin P. Approximate wall boundary conditions in the large eddy simulation of high Reynolds number flow. *Flow, Turbulence and Combustion* 1999; **63**:269–291.
23. Wang M. Dynamic wall modelling for LES of complex turbulent flows. In *Annual Research Briefs*, Center for Turbulent Research, Stanford Univ./NASA Ames Research Center, 2000; 241–250.
24. Wang M, Moin P. Dynamic wall modelling for large eddy simulation of complex turbulent flows. *Physics of Fluids A* 2002; **14**(7):2043–2051.
25. Shur M, Spalart PR, Strelets M, Travin A. Detached-eddy simulation on an airfoil at high angle of attack. In *Engineering Turbulence Modelling and Experiments*, vol. 4, Rodi W, Laurence D (eds). Elsevier: Amsterdam, 1999; 669–678.
26. Constantinescu GS, Squires KD. LES and DES investigations of turbulent flow over a sphere. AIAA 2000-0540, Reno, 1998.
27. Travin A, Shur M, Strelets M, Spalart P. Detached-eddy simulations past a circular cylinder. *Flow Turbulence and Combustion* 2000; **63**(1/4):293–313.
28. Forsythe JR, Hoffmann KA, Dietiker J-F. Detached-eddy simulation of a supersonic axisymmetric base flow with an unstructured solver. AIAA paper 00-2410, Denver, 2000.
29. Strelets M. Detached eddy simulation of massively separated flows. AIAA paper 2001-0879, Reno, NV, 2001.
30. Nikitin NV, Nicoud F, Wasistho B, Squires KD, Spalart P. An approach to wall modeling in large-eddy simulations. *Physics of Fluids A* 2000; **12**(7):1629–1632.
31. Tucker P, Davidson D. Zonal k-l based large eddy simulations. AIAA paper 2003-0082, Reno, 2003.
32. Davidson L, Cokljat D, Fröhlich J, Leschziner MA, Mellen C, Rodi W (eds). *LESFOIL: Large Eddy Simulation of Flow Around a High Lift Airfoil*, vol. 83. Springer: Berlin, 2003.
33. Peng S-H, Davidson L, Holmberg S. A modified low-Reynolds-number $k-\omega$ model for recirculating flows. *ASME: Journal of Fluids Engineering* 1997; **119**:867–875.
34. Yoshizawa A. Bridging between eddy-viscosity-type and second-order models using a two-scale DIA. In *9th International Symposium on Turbulent Shear Flow*, vol. 3, Kyoto, 1993; 23.1.1–23.1.6.

35. Fureby C. Large eddy simulation of rearward-facing step flow. *AIAA Journal* 1999; **37**(11):1401–1410.
36. Davidson L, Peng S-H. A hybrid LES-RANS model based on a one-equation SGS model and a two-equation $k-\omega$ model. In *The Second International Symposium on Turbulence and Shear Flow Phenomena*, vol. 2, Lindborg E, Johansson A, Eaton J, Humphrey J, Kasagi N, Leschziner M, Sommerfeld M (eds). Stockholm, 2001; 175–180.
37. P. Emvin. The full multigrid method applied to turbulent flow in ventilated enclosures using structured and unstructured grids. *PhD Thesis*, Dept. of Thermo and Fluid Dynamics, Chalmers University of Technology, Göteborg, 1997.
38. L. Davidson. MTF071 Computational Fluid Dynamics of turbulent flow. Lecture notes, www.tfd.chalmers.se/gr-kurs/MTF071, Dept. of Thermo and Fluid Dynamics, Chalmers University of Technology, Göteborg, Sweden, 2000.
39. Rhie CM, Chow WL. Numerical study of the turbulent flow past an airfoil with trailing edge separation. *AIAA Journal* 1983; **21**:1525–1532.
40. U. Piomelli. High Reynolds number calculations using the dynamic subgrid-scale stress model. *Physics of Fluids A* 1993; **5**:1484–1490.
41. Mellen C, Fröhlich J, Rodi W. Karlsruhe's mid-term report, LESFOIL: A Brite-Euram project. *Technical Report*, Institut für Hydrodynamik, University of Karlsruhe, Germany, 1999.
42. Mellen CP, Fröhlich J, Rodi W. Large eddy simulation of the flow over periodic hills. In *16th IMACS World Congress 2000*, Lausanne, August 21–25, 2000.
43. Temmerman L, Leschziner MA. Large eddy simulation of separated flow in a streamwise periodic channel constriction. In *The Second International Symposium on Turbulence and Shear Flow Phenomena*, vol. 3, Stockholm, 2001; 399–404.
44. Davidson L. Hybrid LES-RANS: A combination of a one-equation SGS model and a $k-\omega$ model for predicting recirculating flows. In *ECCOMAS CFD Conference*, Swansea, U.K., 2001.
45. Temmermann L, Leschziner MA, Hanjalic K. A-priori studies of near-wall RANS model within a hybrid LES/RANS scheme. In *Engineering Turbulence Modelling and Experiments*, vol. 5, Rodi W, Fureby N (eds). Elsevier: Amsterdam, 2002; 17–326.
46. Ghosal S, Moin P. The basic equations for the large eddy simulation of turbulent flows in complex geometry. *Journal of Computational Physics* 1995; **118**:24–37.
47. Dahlström S. Large eddy simulation of the flow around a high-lift airfoil. *PhD Thesis*, Dept. of Thermo and Fluid Dynamics, Chalmers University of Technology, Göteborg, Sweden, 2003.
48. Dahlström S, Davidson L. Hybrid RANS–LES with Additional Conditions at the Matching Region, to be presented at the *Int. Symp. on Turbulence, Heat and Mass Transfer*, Antalya, Turkey, 2003.